 FDMP, vol.1, no.3, pp.247-266, 2005

A Model for Electromagnetic Control of Buoyancy Driven Convection in Glass Melts

C. Giessler [1], C. Sievert [2], U. Krieger [1], B. Halbedel [1], D. Huelsenberg [1], U. Luedke [2], A. Thess [1,2,3]

Abstract: Buoyancy driven motion of a highly viscous electrically conducting fluid under the influence of Lorentz forces is investigated theoretically and experimentally. This problem is relevant to the processing of glass, where it is of considerable interest to know whether electromagnetic forces can effectively improve mixing and help to avoid undesired flow patterns in glass melting furnaces. Two highly simplified models are proposed in which the fluid is assumed to be confined in a circular loop containing several localized resistive heating, convective cooling, and electromagnetic forcing elements. The first model is used to derive the scaling laws of the mean velocity and maximum temperature depending on the electric current density and magnetic field. The predictions of this model are found to be in agreement with numerical simulations and with experiments in a small-scale glass melting furnace. Using the second model which contains two cooling elements we demonstrate that the steady-state velocity in the general case is determined by a single nonlinear algebraic equation whose bifurcation structure reveals an unexpectedly subtle influence of the Lorentz force on buoyancy driven convection. It is shown that the system undergoes a transition from a nearly stably stratified "slow" mode for weak Lorentz forces, in which the velocity v and temperature θ_H scale with the electric current density J_0 as $v \sim const.$ and $\theta_H \sim J_0^2$ to a "fast" mode for strong Lorentz forces in which the scaling on the magnetic field B_0 is $v \sim J_0 B_0$ and $\theta_H \sim J_0^{4/3} B_0^{-2/3}$. In a wide range of parameters this transition depends discontinuously on the magnetic field and has the character of a subcritical bifurcation involving hysteresis. The scaling laws imply that already a comparatively weak electromagnetic force can strongly modify buoyancy driven convection. The consequences of this finding for electromagnetic control of glass melting processes are briefly discussed.

[1] Department of Mechanical Engineering
[2] Department of Electrical Engineering, Ilmenau University of Technology, P. O. Box 100565, 98684 Ilmenau, Germany
[3] corresponding author: thess@tu-ilmenau.de

1 Introduction and technical background

Glass is a ubiquitous material whose reliable production requires a comprehensive understanding and accurate prediction of its flow when it is in its liquid phase at temperatures between 1200^oC and 1600^oC . Although there have been intensive efforts in the glassmaking industry (Krause & Loch 2002) and from the side of commercial computational fluid dynamics (CFD) software developers (Prasad et al 1999) to implement and exploit numerical models of glass flows in melting furnaces, the underlying fluid dynamical problem - mixed convection of a high-Prandtl number fluid with internal heat generation at high Rayleigh and low Reynolds numbers - remains poorly understood. This is particularly true for all-electric furnaces where the flow is driven by the combined action of (Joule-heat-induced) buoyancy and Lorentz forces. In this case there is a long-standing and still unresolved controversy (Hofmann & Philip 1992, Choudhary 1995, Hofmann & Thess 2002) as to whether naturally occuring electromagnetic forces should be included into numerical models of glass melt flows. Moreover, one would like to know whether additional Lorentz forces, created by applying external magnetic fields, can lead to sufficiently strong changes in the flow velocity (which usually is of the order of a couple of millimeters per second) so as to enhance mixing and to avoid undesired flow patterns. While the application of electromagnetic fields for flow control in other areas of materials processing like semiconductor crystal growth, steel casting, and production of aluminium is a well established technique based on a good understanding of the underlying fluid dynamical phenomena (Davidson 1999, Davidson 2001, Davidson & Lindsay 1998), the application of electromagnetic fields to glass melts is a comparatively new topic. The difficulty with glass melts arises from the fact that their electrical conductivity is nearly than five orders of magnitude smaller than that of liquid metals. The goal of the present work is to formulate a conceptually simple model which displays the delicate interplay

between buoyancy, viscous friction, and Lorentz forces in its purest form and permits one to systematically investigate how strong electromagnetic forces ought to be in order to effectively control the flow of a glass melt. The present model should be considered as a prologue to a comprehensive analysis of electromagnetic forces in glass melts because it does not take into account the dependence of viscosity and electrical conductivity on temperature and the heat transfer by radiation.

The paper is organized as follows. With the detailed explanation of the technical background we pave the ground for the definition of our family of models which shall be formulated in section 2. Section 3 contains an analysis of the simplest representative of this family, referred to as model A, which is embodied in eq. (33). This model is amenable to fully analytic treatment and is compared with numerical simulations and laboratory experiments but does not represent the most general case. In section 4 we analyze a slightly more realistic model, called model B, which is described by eq. (45). This model displays the non-monotonic action of the magnetic field. Section 5 summarizes our conclusions and translates our findings into general scaling laws which are believed to provide a rational framework for the application of Lorentz forces to control glass melt flows.

Fig. 1 shows a highly simplified picture of an all-electric furnace for glass melting. An alternating electric current of about 1000 Ampere is injected into the electrically conducting highly viscous glass melt using two or more electrodes. This electric current has three effects, namely (i) resistive heating of the melt, (ii) creation of buoyancy, (iii) generation of a Lorentz force. Heating and buoyancy is a result of the volumetric heat production

$$q = \frac{\mathbf{J}^2}{\sigma} \tag{1}$$

where $\mathbf{J}(\mathbf{x},t)$ is the electric current density and σ the electrical conductivity of the melt. Glass melts are poor electric conductors with conductivities of the order $\sigma \approx 10\Omega^{-1}m^{-1}$ as compared with $\sigma \approx 10^6\Omega^{-1}m^{-1}$ for liquid metals and molten semiconductors. The origin of the Lorentz force may be twofold. On the one hand, the electric current in the electrodes, and in the busbar system creates its own magnetic field $\mathbf{b}(\mathbf{x},t)$ determined by Ampere's law $\mu_0\mathbf{J} = \nabla\times\mathbf{b}$ and by $\nabla\cdot\mathbf{b} = 0$. This field results in a "natural" Lorentz force

$$\mathbf{f} = \mathbf{J}\times\mathbf{b} \tag{2}$$

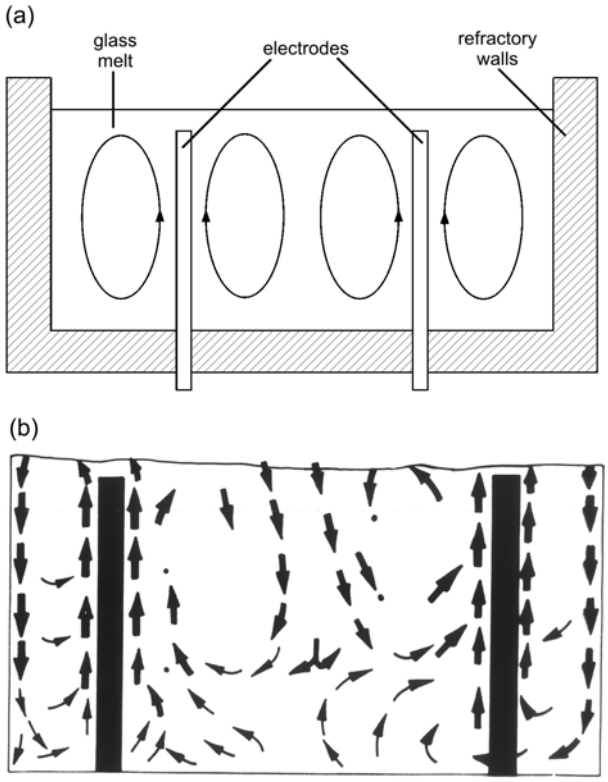

Figure 1 : Convection in an all-electric glass furnace: (a) Schematic of the furnace and of the flow field, (b) measured velocity distribution in an industrial all-electric furnace (reproduced from Illig et al 1978). Observe that a fluid element traveling along one of the streamlines shown, will experience a Joule heating during its upward motion followed by radiative cooling at the free surface and a conductive cooling at the refractory walls. The primary source of convective motion is buoyancy due to Joule heating, but the flow is also affected by "natural" Lorentz forces generated in the vicinity of the electrodes as descibed in the text.

which is always present in all-electric melting furnaces and was studied by Hofmann & Philip 1992 and Choudhary 1996. Similar flows occur in a variety of electromagnetic materials processing techniques and are often called electrically induced vortical flows (Bojarevics et al 1988). On the other hand, since the pioneering work of Osmanis and co-workers (Osmanis et al 1987), there has been a growing interest in the application of external magnetic fields $\mathbf{B}(\mathbf{x},t)$ in order to create additional "artificial" Lorentz forces

$$\mathbf{f} = \mathbf{J}\times\mathbf{B} \tag{3}$$

so as to intensify mixing, which is crucial in the production of high-homogeneity glasses for optical applications.

The challenge in any practical application is to predict the velocity and temperature distribution of the liquid glass in the melting volume for a prescribed set of geometry parameters, electric current, and magnetic field distributions. More precisely, one would generally like to answer the following two questions: Is it necessary to take into account the natural Lorentz forces [cf. eq. (2)] when performing numerical simulations of glass melt flows in all-electric furnaces? How strong should an artificial Lorentz force [cf. eq. (3)] be in order to rearrange the flow in some predetermined manner? Up to now, the influence of Lorentz forces on glass melt flows was not systematically explored. It was generally believed that the effect of Lorentz forces is a linear one in the sense that the increase in stirring velocity Δv due to a Lorentz force f is of the order $\Delta v \sim f$. We are not able to address the foregoing questions in their full generality, as this would involve the consideration of an infinite variety of possible configurations of electric current and magnetic field distributions. We shall rather limit the scope of our work to the search for a physical mechanism which involves a non-trivial action of a Lorentz force upon a convective flow. Our model, to be defined below, shows indeed that Lorentz forces affect buoyancy driven convection in a very subtle way, and that under appropriate circumstances small changes in f may lead to drastic increases of the flow velocity.

Our model shown in Fig. 2, is inspired by early (Keller 1966, Welander 1967, Creveling et al 1975) and more recent work (Davis & Roppo 1987, Yorke et al 1987, Ehrhard et al 1989, Ehrhard & Müller 1990) modelling thermal convection by the motion of a fluid in a closed vertical loop as well as by the recent progress in the application of scaling and similarity theory to the description of thermal convection at high Rayleigh number (Siggia 1994, Grossmann & Lohse 2000, 2003).

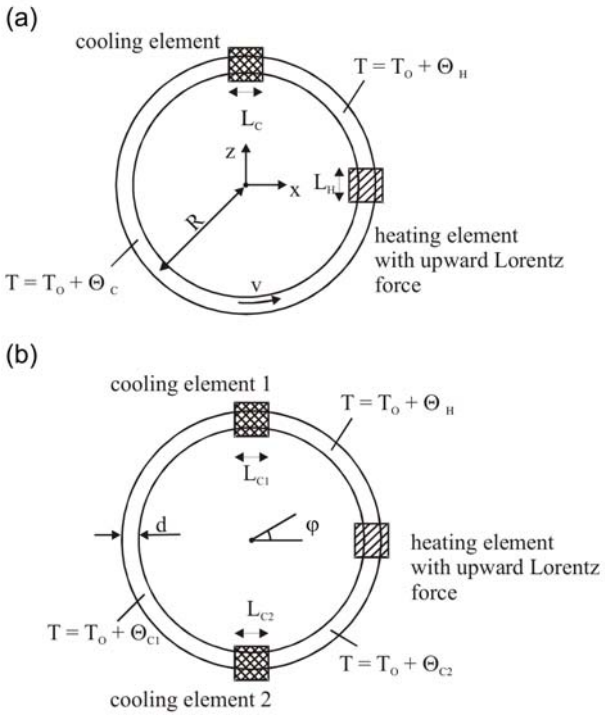

Figure 2 : Sketch of the considered models: (a) circular loop with one cooling element (model A), (b) circular loop with two cooling elements (model B). Both, the electric current and the magnetic field are assumed to be time independent (DC). Notice, however, that in industrial practice AC current with a frequency of 50Hz is used in order to avoid electrolysis in the glass melt and that the applied magnetic field (if any) must oscillate with the same frequency in order to produce a Lorentz force with non-zero mean value. Since the time scales of oscillation of the heat flux and the Lorentz force are much smaller than the time scales of the flow, only their mean values are of importance.

2 Formulation of the problem and general considerations

2.1 Definition of the considered system

Let us consider a circular loop filled with a fluid with kinematic viscosity ν, thermal diffusivity κ, coefficient of thermal expansion α, density $\rho = \rho_0[1 - \alpha(T - T_0)]$, and electrical conductivity σ. Since the Prandtl number $Pr = \nu/\kappa$ of glass melts is of the order 10^3, we shall assume $Pr \gg 1$. We take into account that ν, κ, α, and σ are functions of temperature but neglect their variation within the loop in order to keep the model as simple as possible. However, the reader should have in mind that in real glass melts ν and σ can vary by orders of magnitude and that these variations give rise to strong nonlinear effects such as thermal runaway and freezing instabilities (Lange & Loch 2002). Similar effects are known to occur in lava flows, which have been investigated by Wylie & Lister (1995, 1998). Our neglect of viscosity and con-

ductivity variations within the loop should therefore be considered as a preliminary measure which is taken in order not to obscure the interaction between Lorentz forces and buoyancy.

As shown in Fig. 2, the fluid is heated by passing a homogeneous electric current $\mathbf{J} = J_0\mathbf{e_x}$ through it, applied over a section with length L_H which delivers a volumetric heat generation rate $q = J_0^2/\sigma$ to the fluid. At the same time a magnetic field $\mathbf{B} = B_0\mathbf{e_y}$ is assumed to act upon the heating section. At this point we do not distinguish between natural and artificial Lorentz force and suppose that B_0 and J_0 are independent input parameters, even though B_0 may depend on J_0. The resulting Lorentz force density $\mathbf{f} = J_0B_0\mathbf{e_z}$ drives the fluid in counterclock wise direction. The Lorentz Forces are concentrated near by the electrodes. The reason is the decreasing electrical field density by increasing distance according $J \sim r^{-1}$ for rod electrodes and $J \sim r^{-2}$ for point electrodes. This relations allow us to concentrate the Lorentz Force at the heating section. In addition to the Lorentz force, a buoyancy force is generated due to the nonuniform distribution of temperature which results from cooling the fluid. We shall consider two models, referred to as model A and model B, characterized by one and two cooling sections respectively. Model A is the simplest nontrivial system, while model B is a more general caricature of the original system shown in Fig. 1 in that it takes into account both cooling at the free surface and at the sidewalls. In general, the model might be formulated for any position of the heating and cooling sections. The position of the cooling sections of model B is applicable for internal vortices which do not meet the side walls. This specific kind of vortices appears between two inner rod electrodes of a rod electrode line immersed into a glass melt furnace. Cooling in our model is accomplished by exposing the walls of the loop to a prescribed ambient temperature T_0 along the cooling elements. The remaining portions of the wall are assumed adiabatic. It is convenient to write the temperature as $T = T_0 + \theta$ and to formulate the theory in terms of the temperature deviation θ.

For prescribed values of J_0, B_0, T_0, and a given set of material and geometry parameters, the goal of our theoretical model is to predict the velocity v and temperatures θ_H and θ_C [θ_H, θ_{C1}, and θ_{C2}] for model A [model B] in a steady state. The velocity is related to the volume flux Q through the cross-sectional area A of the pipe by $v = Q/A$ and is assumed to be the same at all points of the fluid.

Our model is based on two ingredients namely (i) the balance of torques acting on the fluid, expressed by

$$\mathbf{0} = \Sigma_V + \Sigma_B + \Sigma_L \tag{4}$$

where Σ_V is the viscous torque, Σ_B the buoyancy torque and Σ_L the Lorentz torque, respectively and (ii) a set of constitutive relations of the form

$$\theta_C = f(v)\theta_H, \quad \theta_H = \theta_C + g(v) \quad [for\ \ model\ \ A] \tag{5}$$

$$\theta_{C1} = f_1(v)\theta_H, \quad \theta_{C2} = f_2(v)\theta_{C1}, \quad \theta_H = \theta_{C2} + g(v) \quad [for\ \ model\ \ B] \tag{6}$$

where the functions $f(v)$ and $g(v)$ describe the relation between the temperatures of the fluid entering and leaving the heating or cooling section. A number of properties of the systems can be deduced from very general qualitative considerations without any reference to the specific form of these functions, as will be shown next.

It is readily verified that the torque on the fluid is in the y-direction and can therefore be expressed as $\Sigma = -\Sigma\mathbf{e}_y$. For flows at low Reynolds number, such as glass melt flows, the viscous torque must be of the form

$$\Sigma_V = -\mu v \tag{7}$$

where the friction coefficient μ depends on the shape of the cross-section and on the viscosity, as will be described in detail in section 3. The buoyancy torque is written as

$$\Sigma_B = \beta(v) \tag{8}$$

where the function $\beta(v)$ depends on the properties of the heating and cooling system as well as on the (unknown) velocity. The shape of $\beta(v)$ will be separately discussed for models A and B below. Finally, the Lorentz torque can be expressed as

$$\Sigma_L = \gamma \tag{9}$$

were $\gamma \sim J_0B_0$ describes the strength of the Lorentz force. As a result, the velocity is determined by the non-linear equation

$$\mu v = \beta(v) + \gamma \tag{10}$$

The family of steady solutions $v(\gamma)$ of this equation can be qualitatively understood by tracing the intersection between the functions μv and $\beta(v) + \gamma$ once the shape of $\beta(v)$ is known.

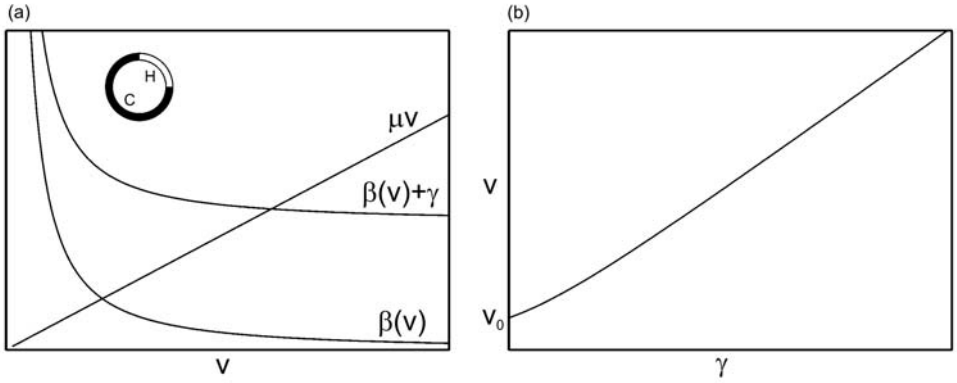

Figure 3 : General behaviour of model A: (a) Graphic solution of eq. (10) together with a sketch of the steady state velocity depending on the Lorentz force (b)

2.2 General properties of steady states

Consider first model A, characterized by a single cooling element. The heat taken up by each fluid element is proportional to the volumetric rate of Joule heat production J_0^2/σ and to the time L_H/v necessary to traverse the heating element. Consequently, the temperature difference $\theta_H - \theta_C$ is a decreasing function of v. Moreover, the spatial distribution of hot (light) and cold (heavy) fluid which determines the sign of $\beta(v)$ is always the same because the system is always top-heavy with cold fluid corresponding to unstable stratification. As a result, $\beta(v)$ is a monotonically decreasing function of v whose qualitative shape is shown in Fig. 3a.

For $\gamma = 0$ its intersection with μv defines a velocity scale v_0 characterizing the intensity of the nonmagnetic flow. As γ is increased, the intersection is displaced to the right and the velocity is a monotonically increasing function of the Lorentz force as shown in Fig. 3b. However, model A does not represent the most general case because the fluid is always unstably stratified.

Model B is the simplest variant of the generic case including the possibility of transition from unstable to stable stratification. This system is characterized by the presence of two cooling elements. Assume for a moment that v were known and let us derive, from general considerations, the shape of $\beta(v)$. For low velocities the first cooling section will be very effective in cooling the fluid down to a low temperature. Therefore the temperature distribution will be virtually the same as in model A (cf. insert 1 in Fig. 4a) and $\beta(v)$ will decay as shown in Figs. 4a and c for $v \to 0$. However, as v is increased, the first cooling section becomes less effective and warm fluid invades the left part of the annulus before it is completely cooled down by the second cooling section.

There is some velocity at which the total torque becomes zero, as shown in inset 2 of Fig. 4a. Further increase of v leads to a reversal of the sign of $\beta(v)$ (cf. insert 3 of Fig. 4a) which, for $v \to \infty$, tends to zero. For low electric current $\beta(v)$ sketched in Fig. 4a is smaller and less steep than for higher current, shown in Fig. 4c. This behavior is based on the fact, that the heat generation is proportional to J_0^2. For increasing velocities and higher electrical current the reduction of generated heat and therefore the reduction of $\beta(v)$ is greater than for smaller electrical current. It turns out that there exists a critical electric current I_c which strongly affects the behavior of the system once the Lorentz force is switched on. For $I < I_c$ there is a unique intersection between μv and $\beta(v)$ as seen in Fig. 4a which leads to a monotonic function $v(\gamma)$ shown in Fig. 4b. When $I > I_c$ there are multiple intersections (cf. Fig. 4c) implying that there is a jump in the velocity once γ is increased beyond a critical value. This transition involves hysteresis, as demonstrated in Fig. 4d.

2.3 Specification of the heat transfer models

Before proceeding to an analysis of both systems we need to supply our model with specific functions $f(v)$ and $g(v)$.

To derive the cooling function $f(v)$ we observe that the Peclet number $Pe = vd/\kappa$ in glass melt flows is usually high. We therefore assume that the passage of the hot fluid with $\theta = \theta_H$ along the cold isothermal wall with $\theta = 0$ results in a thermal boundary layer, shown in Fig.

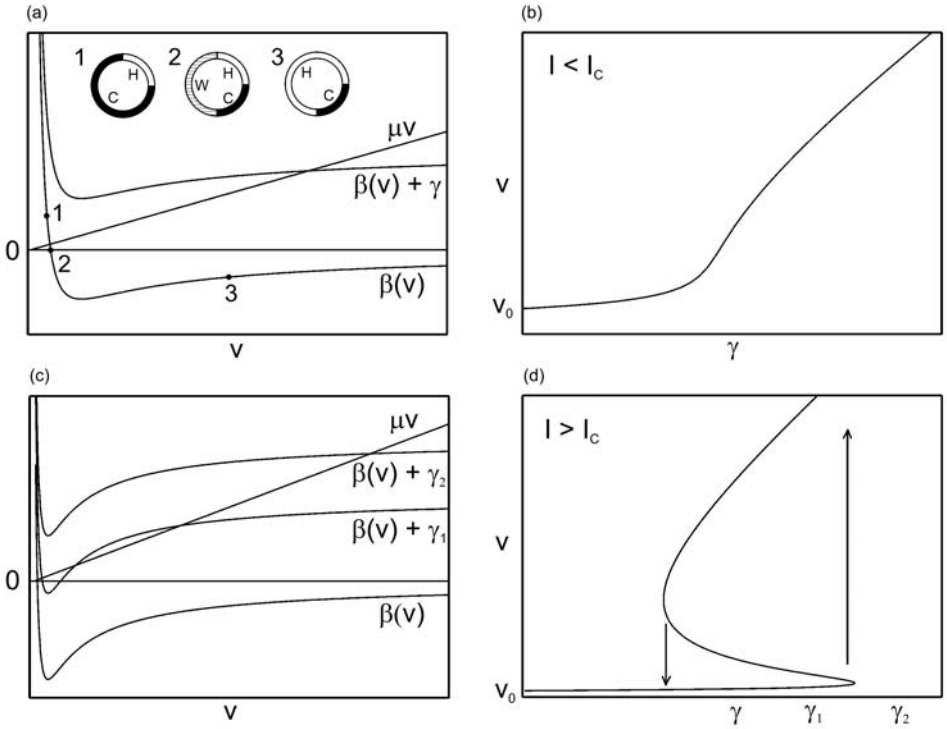

Figure 4 : General behaviour of model B: (a), (c) Graphic solutions of eq. (10) together with a sketch of the steady state velocities depending on the Lorentz force (b), (d). The case $I < I_c$ with continuous parameter dependence is shown in (a) and (b) while the case $I > I_c$ exhibiting jumps and hysteresis is shown in (c) and (d). Insets in (a) show the distribution of hot (H), warm (W), and cold (C) fluid corresponding to points 1,2, and 3 of the curve $\beta(v)$.

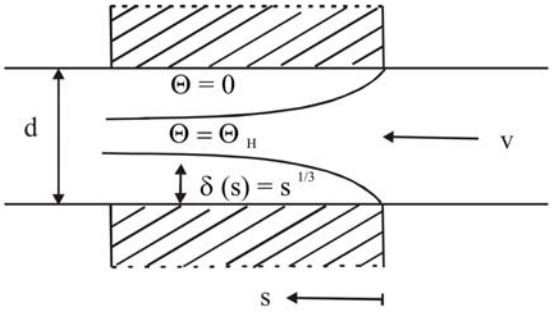

Figure 5 : Structure of the thermal boundary layer in the cooling section.

5, whose thickness evolves as

$$\delta(s) = c_T \left(\frac{\kappa s}{\tau}\right)^{1/3} \tag{11}$$

which is typical of high-Prandtl-number fluids (Shraiman & Siggia 1990, Wylie & Lister 1995, Ching 1997). Here s is the arc-length, κ the thermal diffusivity of the fluid, $\tau = dv_t/dn$ the wall-normal gradient of the tangential velocity, and c_T a numerical constant of order one. We parenthetically note that this boundary layer structure also underlies the empirical relations for estimating mixing and homogenization times in glass processing (Beerkens 2002). For high Peclet numbers i.e. $Pe = vd/\kappa \gg 1$ the mean (cross-section averaged) temperature $\theta(s)$ is a weighted average between $\theta = \theta_H$ and $\theta = 0$ in the form

$$\theta(s) = \left[1 - \frac{2\delta(s)}{d}\right] \theta_H \tag{12}$$

For high Peclet numbers the heat transfer by conduction is small in comparison with convection and radiation. To keep the model simple the internal heat transfer by radiation is not included, but can be phenomenologically taken into account using an enhanced heat diffusivity. It should be mentioned that the Peclet number should not be too large to prevent the temperature to become uniform after passing the cooling element and before entering the heating section.

With eq. (12) $\theta_c = \theta(L_c)$ can be expressed as soon as τ is known. For general flows $\tau = c_f(v)v^2/2\nu$ can be expressed using the friction factor $c_f(v)$ (White 2002).

For laminar flows we have $c_f = c_V/Re$ (e.g. $c_V = 16$ for laminar flow in a circular pipe) leading to $\tau = c_V \nu/2d$ and thus to

$$f(v) = 1 - \left(\frac{16\kappa c_T^3 L_c}{c_V \nu d^2}\right)^{1/3} \tag{13}$$

For $v \to \infty$ we have $f \to 1$ implying that the temperature is unchanged. For $v \to 16\kappa L_c/c_V d^2$, on the other hand, $f \to 0$, i.e. the fluid is cooled down to the lowest possible temperature $\theta = 0$. In addition to that we assume that $f = 0$ for $v < 16\kappa L_c/c_V d^2$. However, this case is of no importance here, since it corresponds to low Peclet numbers while we are interested in $Pe \gg 1$ here.

The heating function $g(v)$ is derived from the observation that a fluid element moving through the electric heating section obeys

$$c_p \rho_0 v \frac{d\theta}{ds} = \frac{J_0^2}{\sigma} \tag{14}$$

where c_p is the specific heat of the fluid. This equation is easily integrated over the heating section $-L_H/2 \le s \le +L_H/2$ using the boundary condition $\theta(-L_H/2) = \theta_C$ to obtain $\theta_H \equiv \theta(+L_H/2)$ as

$$\theta_H = \theta_C + \frac{J_0^2 L_H}{c_p \rho_0 \sigma v} \tag{15}$$

Thus we have

$$g(v) = \frac{J_0^2 L_H}{c_p \rho_0 \sigma v} \tag{16}$$

which decreases as $1/v$ as expected from our general discussion.

The constitutive relations can now be written in a compact form as

$$f(v) = 1 - \left(\frac{v_*}{v}\right)^{1/3} \tag{17}$$

$$g(v) = \theta_* \frac{v_*}{v} \tag{18}$$

With

$$v_* = \frac{16\kappa L_c c_T^3}{c_V d^2} \tag{19}$$

$$\theta_* = \frac{J_0^2 L_H c_V d^2}{16 c_p \rho_0 \sigma \kappa L_c c_T^3} \tag{20}$$

For model B we have two velocities v_{*1}, and v_{*2}, evaluated with L_{C1} and L_{C2} respectively, and $g(v)$ should be computed using $L_C = L_{C1}$. Finally we shall need the expressions for the temperatures in terms of f and g. They are readily derived from eqn. (2.2) and (2.3) as

$$\theta_H = \frac{g}{1-f}, \quad \theta_C = \frac{fg}{1-f} \tag{21}$$

and

$$\theta_H = \frac{g}{1-f_1 f_2}, \quad \theta_{C1} = \frac{f_1 g}{1-f_1 f_2} \quad \theta_{C2} = \frac{f_1 f_2 g}{1-f_1 f_2} \tag{22}$$

3 Analysis for the case of a single cooling element

3.1 *Mathematical model and nondimensional variables*

We apply the general theory first to analyze model A, a laminar flow in a loop with circular cross section, small diameter ($d \ll R$), and a single cooling element as shown in Fig. 2a.

The viscous torque $\Sigma_V = RF_V$ can be computed from the force $F_V = 16\pi^2 \rho_0 \nu R v$ acting on the wall of a straight pipe whose length is equal to the circumference $2\pi R$ of our loop assuming a Poiseuille velocity profile. We thus obtain

$$\mu = 16\pi^2 R^2 \rho_0 \nu \tag{23}$$

for the friction coefficient defined in eq. (7).

To compute the buoyancy torque we start from the equation

$$\Sigma_B \equiv \beta(v) = \frac{\pi}{4} d^2 R^2 \rho_0 \alpha g \int_0^{2\pi} \theta(\phi) cos(\phi) d\phi \tag{24}$$

valid for any temperature distribution $\theta(\phi)$ in a circular loop. In order to simplify the analysis we assume that both the heating and cooling sections are very short, i.e. $L_H \ll R$, $L_C \ll R$. Then we can compute the integral as if the temperature distribution were given by

$$\theta(\phi) = \theta_H \quad (0 \le \phi < \pi/2) \tag{25}$$

$$\theta(\phi) = \theta_C \quad (\pi/2 \le \phi < 2\pi) \tag{26}$$

The result $\beta(v) = \pi d^2 R^2 \rho_0 \alpha g (\theta_H - \theta_C)/4$ can be rewritten using eq. (21) and takes the form

$$\beta(v) = \frac{\pi}{4} d^2 R^2 \rho_0 \alpha g \theta_* \frac{v_*}{v} \tag{27}$$

As expected from Fig. 3a, $\beta \sim v^{-1}$.

The third ingredient, namely the electromagnetic torque $\Sigma_L = RF_L$ is readily computed from the Lorentz force $F_L = \pi d^2 L_H J_0 B_0/4$ acting on the fluid in the heating section. As a result we have

$$\gamma = \frac{\pi}{4} R d^2 L_H J_0 B_0 \tag{28}$$

The explicit expressions for μ, β,and γ can now be inserted into (2.7) and we obtain the desired equation

$$16\pi^2 R^2 \rho_0 \nu v = \frac{\pi d^2 R^2 \alpha g J_0^2 L_H}{4 c_p \sigma v} + \frac{\pi R d^2 L_H J_0 B_0}{4} \tag{29}$$

for $v(J_0, B_0)$. Once the velocity has been obtained, the temperatures can be evaluated using eq. (21).

The model can be converted into a more compact form by introducing nondimensional velocity and temperature according to

$$v = v_0 V, \quad \theta_H = \theta_0 T_H, \quad \theta_C = \theta_0 T_C \tag{30}$$

where

$$v_0 = \frac{dJ_0}{8}\left(\frac{\alpha g L_H}{\pi \rho_0 \nu c_p \sigma}\right)^{1/2} \tag{31}$$

$$\theta_0 = \left(\frac{64\pi^2 J_0^4 L_H^2 \nu}{\kappa L_C c_T^3 \rho_0^2 c_p^2 \sigma^2 \alpha g}\right)^{1/3} \tag{32}$$

The resulting equations are

$$V^2 = 1 + MV \tag{33}$$

$$T_H = \frac{1}{V^{2/3}} \tag{34}$$

$$T_C = \frac{1}{V^{2/3}}\left[1 - \frac{1}{PV^{1/3}}\right] \tag{35}$$

They contain two dimensionless parameters, namely a modified Peclet number

$$P = d\left(\frac{J_0}{8\kappa L_c c_T^3}\right)^{1/3}\left(\frac{\alpha g L_H}{\pi \rho_0 \nu c_p \sigma}\right)^{1/6} \tag{36}$$

which is a nondimenensional measure of the electric current, and the Lorentz force parameter

$$M = \frac{dB_0}{8R}\left(\frac{L_H c_p \sigma}{\pi \rho_0 \nu \alpha g}\right)^{1/2} \tag{37}$$

which is proportional to the magnetic field. Eqn. (3.11)-(3.13) uniquely determine the velocity and temperatures of the considered system as functions of the control parameters P and M.

3.2 Solution

The solution of the governing equation (3.11) is easily found as

$$V = \frac{1}{2}\left(M + \sqrt{M^2+4}\right) \tag{38}$$

$$T_H = \left(\frac{2}{M+\sqrt{M^2+4}}\right)^{2/3} \tag{39}$$

$$T_C = \left(\frac{2}{M+\sqrt{M^2+4}}\right)^{2/3} \times \left\{1 - \frac{1}{P}\left[\frac{2}{M+\sqrt{M^2+4}}\right]^{1/3}\right\} \tag{40}$$

These solutions are shown in Fig. 6. In the nonmagnetic case $M = 0$ we have $V = 1$, $T_H = 1$, and $\Delta T \equiv T_H - T_C = P^{-1}$ which corresponds to $v \sim J_0$, $\theta_H \sim J_0^{4/3}$, and $\Delta\theta \sim J_0$. Fig. 6 shows that the velocity is a monotonically increasing function of the magnetic field. For sufficiently strong magnetic fields ($M \gg 1$) $V \sim M$, i.e. the flow is proportional to the Lorentz force density ($v \sim J_0 B_0$). At the same time, the Lorentz force leads to an improved heat transfer and thereby to a reduction of the temperature which is expressed by the asymptotic relations $T_H \sim M^{-2/3}$, $\Delta T \sim P^{-1} M^{-1}$ corresponding to $\theta_H \sim J_0^{4/3} B_0^{-2/3}$ and $\Delta\theta \sim J_0 B_0^{-1}$. Let us translate the nondimensional results of Fig. 6 into physical parameters for a low temperature fluid which is often used in "cold" model experiments whose material properties are given in table 1. It can be seen in Fig. 7 that for $B_0 = 0$ the velocity is of the order of 0.1mm/s and increases almost linearly when a magnetic field is applied.

Already a field with moderate strength $B_0 = 0.1T$ can increase the velocity of the high temperature fluid by an order of magnitude and effectively reduces the maximum temperature as shown in Fig. 11. Notice that in the computation of Fig. 7 the values of η and σ of the model substance were taken at the constant reference temperature of 30^{o}C. This is because their temperature-dependence is weak in the considered range of temperatures. By contrast, when applying to our glass melts in section 3.4, η and σ will have to be determined by a self-consistent procedure which takes into account the solutions for Θ_C and Θ_H.

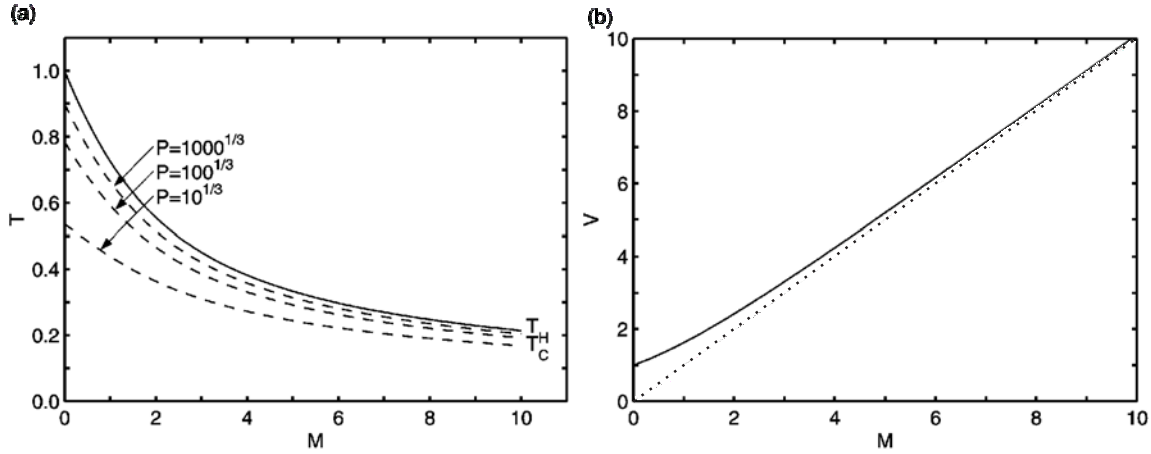

Figure 6 : Solution for nondimensional temperature (a) and velocity (b) in a loop with a single heating and cooling element (model A) as a function of the Lorentz force parameter defined in eq. (36). Notice that v and T_H are independent of P.

Table 1 : Used thermophysical properties of a model substance (Glycerin + LiCl, Stanek 1977) at a reference temperature of 30^oC and a glass melt at a reference temperature of 1180^oC (ρ_0, α) and 1400^oC (c_P), respectivly

Property	Model substance	Glass melt
ρ_0 $[kgm^{-3}]$	1260	3357
η $[Pas]$	0.80	$lg\,\eta = -1.00Pas + \frac{454.36K}{T-1033.41K}$
σ $[\Omega^{-1}m^{-1}]$	0.24	$lg\,\sigma = 6.24\Omega^{-1}m^{-1} - \frac{8.80*10^3K}{T}$
c_P $[Jkg^{-1}K^{-1}]$	2427	1235
α $[K^{-1}]$	$4.80{\cdot}10^{-4}$	$1.18{\cdot}10^{-4}$

3.3 Comparison with numerical simulations

In order to check the validity of our model and to justify its extension to the case of two cooling sections we have performed a series of numerical simulations using the commercial CFD software FLUENT. Rather than solving the three-dimensional pipe-flow problem we have implemented the two-dimensional case corresponding to the flow in a cylindrical gap. Since the latter case differs from the former one only by the value of the coefficient of resistance c_V and the thermal boundary layer parameter c_T (the precise numerical values of which being of no importance for our general conclusions), and since two dimensional flow visualization provides full information on the velocity and temperature fields, this approach was considered more appropriate. We used no-slip boundary conditions for the velocity field and assumed adiabatic sidewalls everywhere except at cooling section where the condition $\theta = 0$ was enforced. The electric current density was held constant at a value of $J_0 = 0.1Acm^{-2}$, while the magnetic field was varied between $B_0 = 0$ and $B_0 = 1T$.

Fig. 8 shows the distributions of temperature perturbation θ and velocity magnitude $v = (v_x^2 + v_y^2)^{1/2}$ for the case $B_0 = 0$ and the material properties corresponding to the room temperature model substance specified in table 1. The global structure of the temperature field agrees well with our assumption [eq. (25) and (26)]. Although the flow is very slow ($v \approx 0.23mm/s$), and the Reynolds number $Re = vd/\nu$ is as small as $Re \approx 3.6 \times 10^{-3}$, the Peclet number $Pe = vd/\kappa \approx 24$ is sufficiently high for a thermal boundary layer to develop in the cooling section. The structure of this boundary layer is clearly visible in the upper inset of Fig. 8a.

The lower inset shows that near-wall fluid elements are heated up over a comparatively short path while particles in the middle of the pipe have to travel over a much longer distance before attaining the high temperature state. This observation is a consequence of the fact that near-wall particles travel slowly and are therefore longer exposed to the resistive heating. Fig. 8b demon-

Table 2 : Comparison of the numerical results for the two-dimensional stationary problem with the analytical results of model A (3.16)-(3.18) for the room temperature model substance. The thermophysical properties are given in table 1. Moreover the following geometry and model parameters were assumed for the numerical simulations: $d = 0.01m$, $R = 0.1m$, $L_H = L_C = 0.01m$, $g = 9.81ms^{-1}$, $c_V = 16$, $c_T = 1$.

Quantity	Analytical result	Numerical result
Θ_H(B=0T) [K]	141	149
Θ_H(B=1T) [K]	123	139
Θ_C(B=0T) [K]	92.3	111
Θ_C(B=1T) [K]	82.4	109
v (B=0T) [mm s^{-1}]	0.227	0.377
v (B=1T) [mm s^{-1}]	0.26	0.475

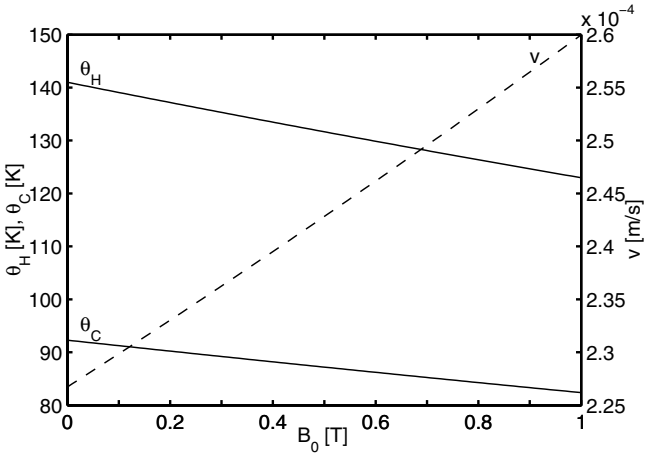

Figure 7 : Solution for dimensional velocity and temperature in a loop with a single heating and cooling element (model A) for a room temperature model substance (Glycerine with LiCl) as a function of the magnetic field. The geometry and material parameters are given in table 1, and $J_0 = 10^4 Am^{-2}$.

strates that the flow is nearly unidirectional everywhere inside the loop except in the immediate vicinity of the heating and cooling sections. Weak deviations from the Poiseuille profile can be readily understood by invoking the relation $\nu\omega_y = \alpha g \partial_x \theta$ for the production of horizontal vorticity by the horizontal temperature gradient in a low Reynolds number flow. In the heating section the temperature decreases as one moves into the fluid, creating two counter rotating vortices which brake the flow in the center of the channel. In the cooling section local vorticity is created which has the same sign as the global rotation of the fluid, leading to a displacement of the velocity maximum towards the upper wall.

When the Lorentz force is switched on, the velocity increases, and the temperatures decrease, but the global appearance of the hydrodynamic fields remains virtually unchanged as compared with Fig. 7. In Table 2 we list selected numerical values and compare them to the predictions of our analytic model. Not only does the theory reflect the qualitative behavior of θ_C and θ_H, but it is also quantitatively similar, which is noteworthy since we have not made any attempt to "tune" the free parameters c_T and c_V.

In summary, the numerical results indicate that our analytical model correctly reflects the physics of the problem and can therefore be used to predict the influence of Lorentz forces on buoyancy driven flows. We parenthetically note that already an extension of the simulations to real glass melts with $\Delta T \sim 100K$ and $R = 1m$ is quite expensive computationally, as it would correspond to a fully time-dependent convection problem at Rayleigh numbers of the order of $Ra \sim 10^{10}$ which is at the limit of current numerical capabilities.

3.4 Comparison with experimental results

Beside the numerical simulations we have developed an experimental setup to investigate the influence of Lorentz forces on the flow of glass melts. Details of the experimental setup and selected results on the influence of the electromagnetic stirring on the homogeneity of the solidified melt have been published by Hülsenberg et al. 2003 and Halbedel et al. 2004. Fig. 9 shows a sketch of the experiment.

The used glass melt consists of 27.1%SiO_2, 47.7%BaO, 20.0%B_2O_3, 5.2%Fe_2O_3 (all data in mass%) with the material properties listed in Table 1. The composition

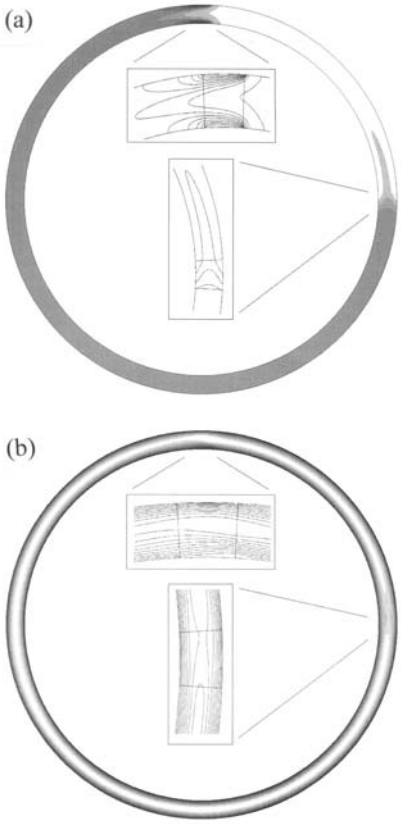

Figure 8 : Temperature and velocity distribution for steady flow in model A at $J_0 = 10^4 Am^{-2}$ as obtained from a two-dimensional numerical solution of the full fluid-dynamical problem without magnetic field. (a) global temperature field with two inserts showing temperature isolines in the vicinity of the heating and cooling section. (b) global representation of the velocity magnitude together with two inserts showing the stream function in the vicinity of the heating and cooling section.

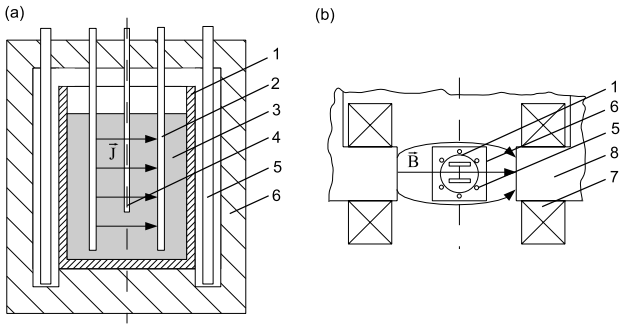

Figure 9 : Schematic diagram of the experimental setup (not to scale) (a) side view showing the predominantly horizontal electric current density, (b) view from above including part of the magnetic system: 1 Pt-crucible, 2 Pt-electrodes, 3 glass melt, 4 thermocouple, 5 heating rods, 6 insulation, 7 coils, 8 yoke of the magnetic system.

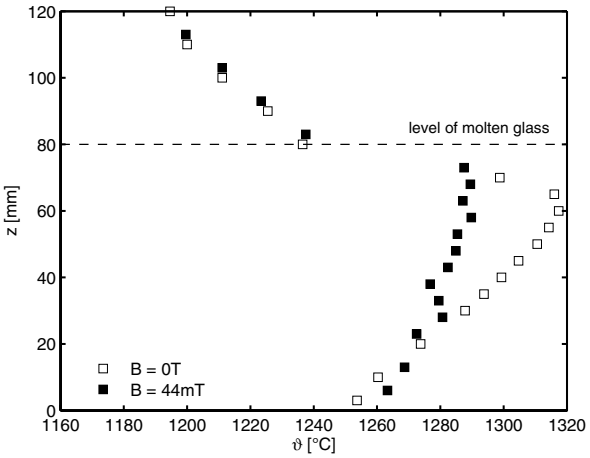

Figure 10 : Experimental results: Temperature distribution along the rotational axis of the crucible without and with external magnetic field.

results in a nearly black glass melt. For this melt the heat transfer by radiation is negligible and therefore agrees with our model property. To avoid contamination as a result of corrosion and to attain high temperature stability the cylindrical crucible consists of oxide dispersion strengthened platinum. The inner diameter of the crucible is $80mm$, the filling height is $80mm$. Two plate electrodes are immersed $60mm$ into the glass melt at a distance of $20mm$ from the axis of symmetry of the cylindrical crucible. An alternating current with a frequency of $50Hz$ results in electrical heating of the glass melt due to the Joule Effect. An external magnetic field with the same frequency is applied perpendicular to the electric current and yields, upon interacting with the electrical current, an upwardly directed Lorentz force between the plate electrodes. The melt cools down at the free surface. Six SiC heating rods are placed axially symmetric around the crucible and provide a highly stable temperature around the crucible. Additional insulation around the whole setup prevents heat loss. This setup leads to an ambient temperature of approximately $T_0 = 1180^oC$. The temperature distribution of the glass melt is measured in situ by a thermocouple, which can be moved along the

rotation axis of the crucible. The measurement of the velocity is not possible due to the high operating temperature. During the experiments a current of $35A$ is applied in combination with an external magnetic field of either $0T$ or $44mT$.

Fig. 10 shows the temperature distribution along the rotational symmetry axis without and with applied external magnetic field. Although we do not have direct access to the velocity field it seems reasonable to assume that the melt rises between the electrodes and falls near the side wall of the crucible. For both cases the glass melt seems to be heated up while ascending along the electrodes and cools down at the free surface. With applied magnetic field the influence of the upward Lorentz force is obvious: the enhanced velocity results in a reduced temperature difference along the rotational axis. Furthermore, the maximum temperature is shifted upward. This is the first direct experimental proof for the homogenizing influence of Lorentz forces on glass melts.

For the analytical calculations the following geometrical parameters are adopted beside the physical properties of the glass melt: the diameter is set to $d = 0.02m$, the radius of the loop is set to $R = 0.08m$ and the length of the cooling and heating zones are set to $L_C = 0.08m$ and $L_H = 0.06m$, respectively. First calculations were performed with a constant viscosity η and a constant electrical conductivity σ of the glass melt for a temperature of 1400^oC. On average the calculated temperatures Θ_C and Θ_H are 15 times higher than the measured ones as seen in Fig. 11a. To understand this apparent discrepancy, let us check if the numerical values of σ and η for the calculated temperature range are consistent with to our given numerical values of $\sigma(T = 1400^oC)$ and $\eta(T = 1400^oC)$. To this end, a definition of mean temperatures is necessary in order to calculate $\sigma(T_\sigma)$ and $\eta(T_\eta)$. The mean temperature of the viscosity is set to $T_\eta = \frac{3}{4}T_C + \frac{1}{4}T_H$ to fulfill the friction distribution over the whole loop. The electrical conductivity influences the heating of the glass melt while passing the heating section. For this reason the average temperature of the heating section $T_\sigma = \frac{1}{2}T_C + \frac{1}{2}T_H$ is used as the mean temperature of σ. As result the electrical conductivity $\sigma(T_\sigma)$ varies between $3.24 \cdot 10^3 \Omega^{-1}m^{-1}$ and $506.54\Omega^{-1}m^{-1}$, the viscosity $\eta(T_\eta)$ varies between $0.16Pas$ and $0.21Pas$, respectively. This comparison indicates, that the model with pre-defined material properties σ and η is "non-self-consistent". To attain a "self-consistent" system the numerical values of σ and η are adopted to the loop temperatures iteratively until the given temperature to determine σ and η are identical to the temperatures calculated with σ and η. Fig. 11b shows the result of the consistent calculations and Table 3 compares the characteristic measured and calculated temperature values. As a result of our self consistent procedure and without tuning the parameters c_T, c_V, c_P and κ the measured temperatures and the calculated ones are now in the same order of amplitude. Furthermore, the experimental setup differs from the analytical model and the internal heat transfer by conduction is neglected. However, the relative temperature changes agree very well and therefore model A describes the main aspects of the experiment quite well. A complete 3D-simulation is in work.

4 Analysis for the case of two cooling elements

4.1 Mathematical model and nondimensional variables

The case of two cooling elements differs from the previous one only in the shape of the buoyancy torque. Using eq. (24) and assuming the temperature field to be of the form

$$\theta(\phi) = \theta_H \quad (0 \le \phi < \pi/2) \tag{41}$$

$$\theta(\phi) = \theta_{C1} \quad (\pi/2 \le \phi < 3\pi/2) \tag{42}$$

$$\theta(\phi) = \theta_{C2} \quad (3\pi/2 \le \phi < 2\pi) \tag{43}$$

we readily obtain $\beta(v) = \pi d^2 R^2 \rho_0 \alpha g(\theta_H - 2\theta_{C1} + \theta_{C2})/4$. With the help of relation (2.19) and the nondimensionalisation

$$v = v_0 V, \quad \theta_H = \theta_0 T_H, \quad \theta_{C1} = \theta_0 T_{C1}, \quad \theta_{C2} = \theta_0 T_{C2} \tag{44}$$

we obtain the following system

$$V^2 = \frac{(P_2 - P_1)V^{1/3} + 1}{(P_2 + P_1)V^{1/3} - 1} + MV \tag{45}$$

$$T_H = \frac{P_2}{V^{1/3}} \frac{1}{(P_1 + P_2)V^{1/3} - 1} \tag{46}$$

$$T_{C1} = \frac{P_2}{V^{1/3}} \frac{1 - P_1^{-1}V^{-1/3}}{(P_1 + P_2)V^{1/3} - 1} \tag{47}$$

$$T_{C2} = \frac{P_2}{V^{1/3}} \frac{(1 - P_1^{-1}V^{-1/3})(1 - P_2^{-1}V^{-1/3})}{(P_1 + P_2)V^{1/3} - 1} \tag{48}$$

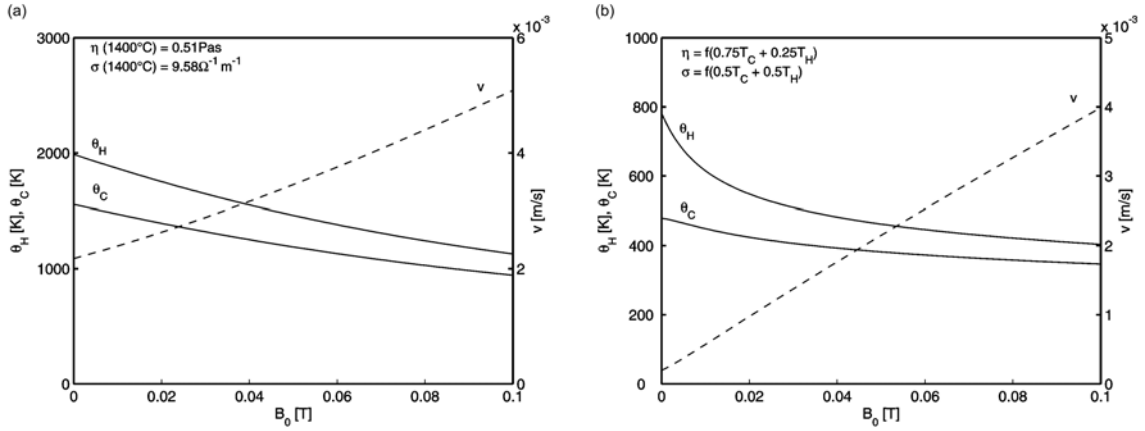

Figure 11 : Solutions for dimensional velocity and temperature in a loop with a single heating and cooling element for the experimentally investigated glass melt as a function of the magnetic field. (a) is a non-self-consistent calculation at a mean melt temperature of 1400^oC while (b) is a self-consistent calculation. The material parameters are given in table 1, the geometry parameters are mentioned in table 3.

Table 3 : Comparison of the results of the self-consistent calculation for model A (3.16)-(3.18) with the experimental results for the glass melt with an ambient temperature of $T_0 = 1180^oC$. In accordance with our experimental setup following geometrical parameters are used for the calculations: $d = 0.02m$, $R = 0.08m$, $L_H = 0.06m$, $L_C = 0.08m$, $g = 9.81ms^{-1}$, $c_V = 16$, $c_T = 1$. Out of the set of measured data the maximum temperature is used to define Θ_H and the temperature at the crucible bottom is used to define Θ_C. The thermophysical properties are given in table 1.

Quantity	Analytical result	Experimental result
Θ_H(B=0T) [K]	781.5	137.4
Θ_H(B=44mT) [K]	473.7	109.8
Θ_C(B=0T) [K]	479.2	73.7
Θ_C(B=44mT) [K]	388.4	83.3
$\frac{\Theta_H}{\Theta_C}$(B=0T)	1.63	1.86
$\frac{\Theta_H}{\Theta_C}$(B=44mT)	1.22	1.32
$\frac{\Theta_H}{\Theta_C}$(B=0T)$-\frac{\Theta_H}{\Theta_C}$(B=44mT)	0.41	0.55
$\frac{\Theta_H(B=0T)}{\Theta_H(B=44mT)}$	1.65	1.25
$\frac{\Theta_C(B=0T)}{\Theta_C(B=44mT)}$	1.23	0.89

which determines the unknown velocity and temperatures. Here P_1 and P_2 are the modified Peclet numbers defined by eq. (36) with L_C replaced by L_{C1} and L_{C2}, respectively. In the interest of clarity, however, we find it more appropriate to write

$$L_{C1} = L_C(1+\varepsilon), \qquad L_{C2} = L_C(1-\varepsilon) \tag{49}$$

in which case P_1 and P_2 can be expressed as

$$P_1 = \frac{P}{(1+\varepsilon)^{1/3}}, \qquad P_2 = \frac{P}{(1-\varepsilon)^{1/3}} \tag{50}$$

where P is given by eq. (36).

Eq. (45)-(48) represent our mathematical model for system B. For a given geometry parameter ε and prescribed electromagnetic control parameters $P \sim J_0^{1/3}$ and $M \sim B_0$ the nonlinear algebraic equation (4.5) determines the velocity $V(\varepsilon,P,M)$ of steady states from which the temperatures $T_H(\varepsilon,P,M)$, $T_{C1}(\varepsilon,P,M)$, and $T_{C2}(\varepsilon,P,M)$ can be explicitly determined. Observe that model A is a particular case of model B corresponding to $\varepsilon \to 1$.

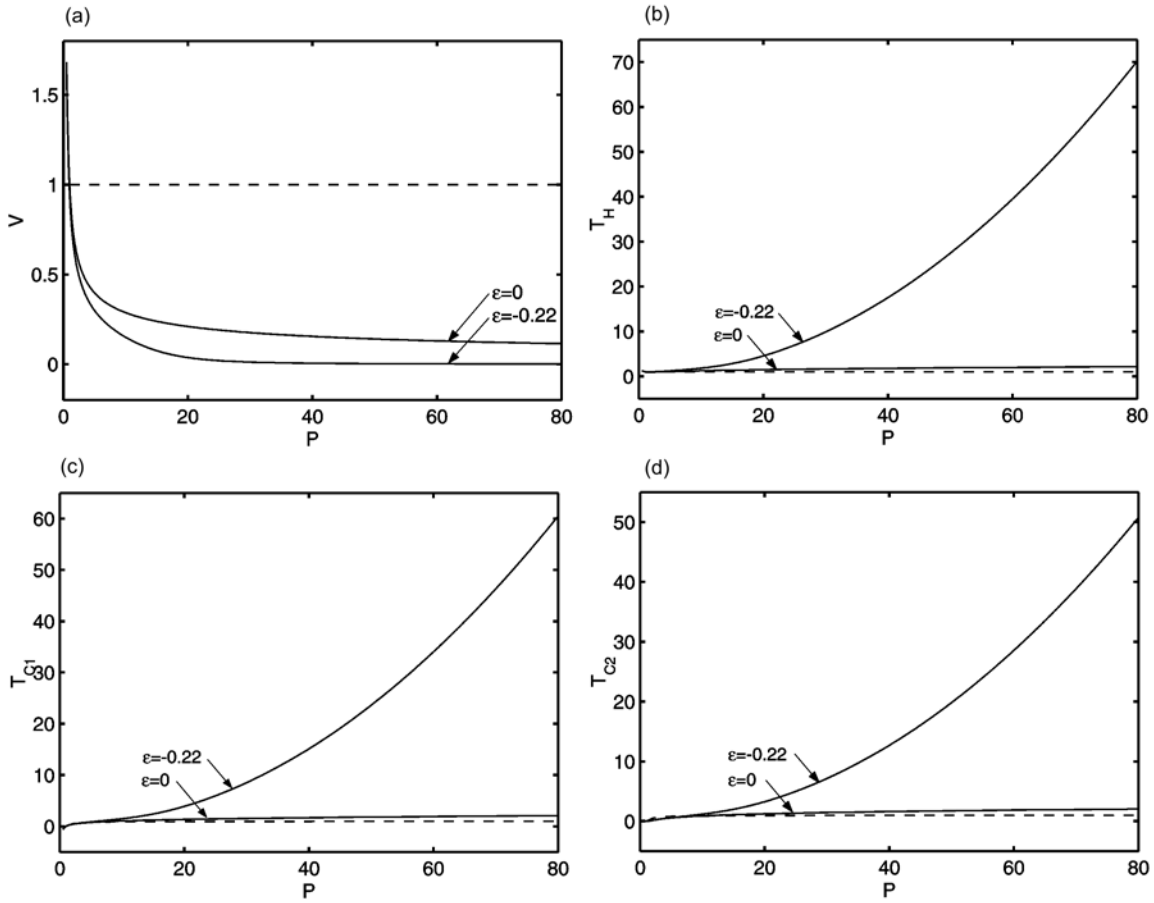

Figure 12 : Solutions for model B in the nonmagnetic case: Velocity (a) and temperatures (b), (c), (d) as obtained by a numerical solution of eq. (45), and eq. (46)-(48) for M=0 with $\varepsilon = 0$ and $\varepsilon = -0.22$. Dashed lines show the nonmagnetic solution of model A for comparison.

4.2 Solution

We start by discussing the nonmagnetic case $M = 0$. Fig. 12 shows numerical solutions corresponding to the case of two cooling sections with equal length ($\varepsilon = 0$), to the case where the lower cooling section is stronger than the upper one ($\varepsilon < 0$) as well as the results for model A. For $\varepsilon = 0$ the velocity is found to decay as $V \sim P^{-3/7}$ which implies that the dimensional velocity scales as $v \sim J_0^{6/7}$ being only slightly different from model A where $v \sim J_0$. This scaling is also easily recovered from the asymptotic behavior of eq. (45) in the limit $P \to \infty$. The slightly slower increase of the velocity in model B as compared with model A is due to the fact that hot fluid can invade the left side of the loop weakening the unstable stratification.

Further qualitative changes occur when $\varepsilon < 0$. As seen in Fig. 12a, the velocity decays much faster than for $\varepsilon = 0$, more precisely as $V \sim P^{-3}$ for $P \gg 1$. This implies $v \to const.$, i.e. the velocity converges to a value independent of the driving electric current. This phenomenon, which we shall refer to as blocking, is a manifestation of the stable stratification already identified in Fig. 4a (inset 2). Mathematically, the zero of the numerator of the first term on the right-hand side of eq. (45) which exists for $P_2 < P_1$ (i.e. $\varepsilon < 0$) implies that the velocity cannot exceed a maximum $V_{max} = (P_1 - P_2)^{-3}$ explaining the observed scaling. It is remarkable that already a slight modification of the geometry parameters can completely change the velocity scaling in thermal convection.

In discussing the behavior of the present system for the general case $M \neq 0$ we shall focus our attention on the case $\varepsilon < 0$ in which a transition from unstable to stable stratification is possible. Fig. 13a-d shows the stationary velocity at different values of P for varying magnetic field. As long as P is below a critical value $P_c(\varepsilon)$, as is

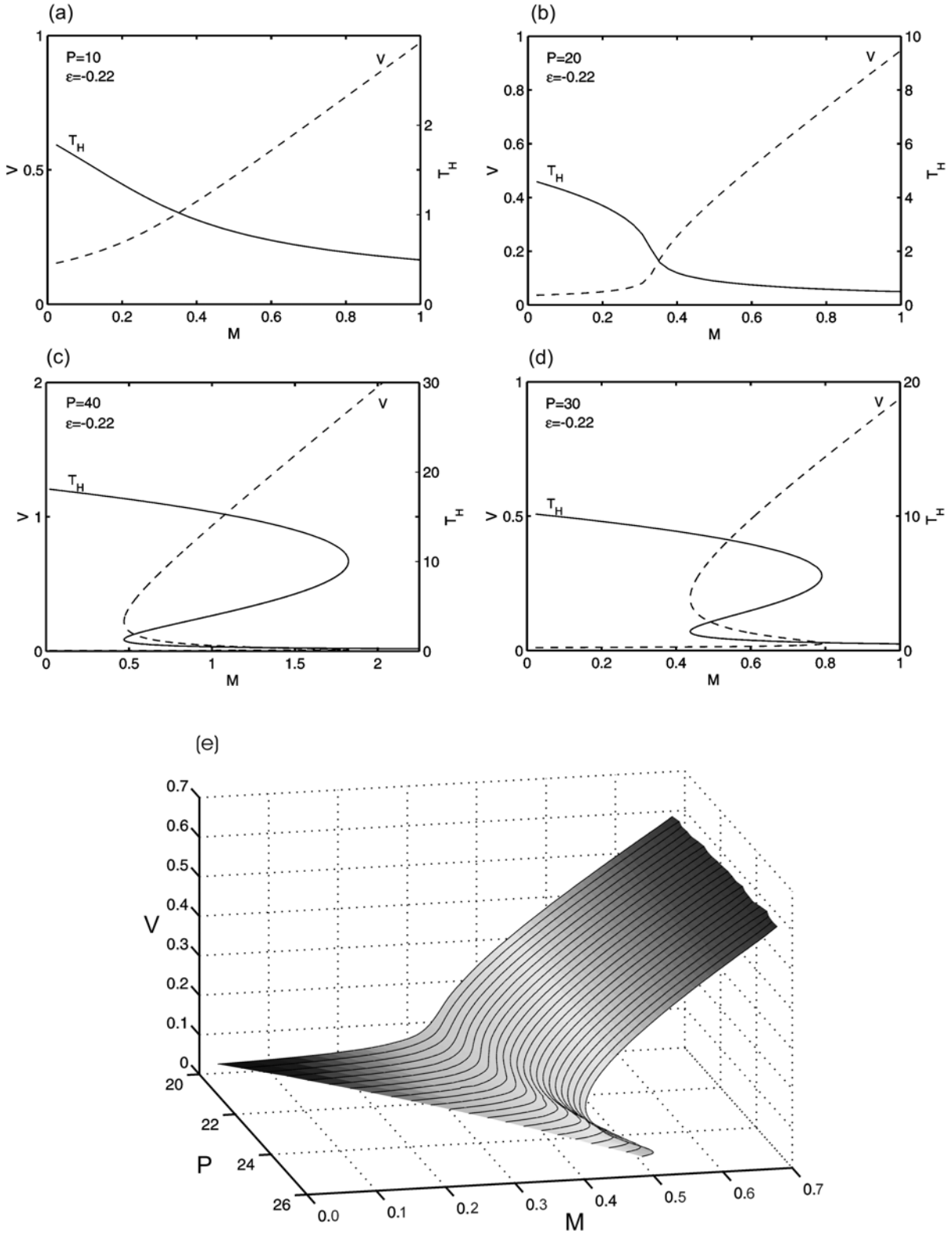

Figure 13 : Solution of model B in the general case for $\varepsilon = -0.22$.

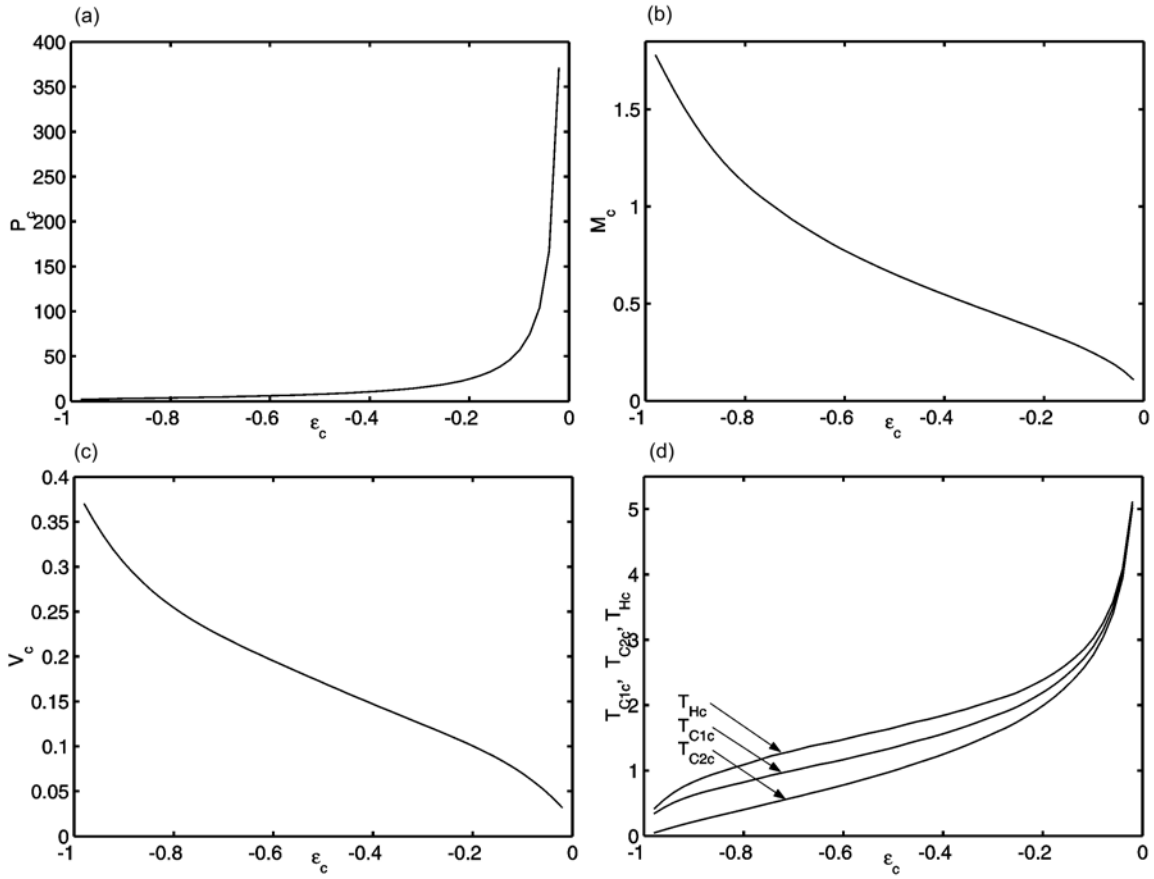

Figure 14 : Location of the critical points $P_c(\varepsilon)$ (a), $M_c(\varepsilon)$ (b), $V_c(\varepsilon)$ (c), $\theta_{Hc}(\varepsilon)$, $\theta_{C1c}(\varepsilon)$, $\theta_{C2c}(\varepsilon)$ as a function of the geometry parameter ε.

the case in Fig. 13a and b, the flow velocity is a monotonically increasing function of M similar to the behavior of model A.

As soon as $P > P_c$ the solution of eq. (45) becomes multiple-valued, i.e. there exist three solutions in an interval $M_- < M < M_+$. To analyze the stability of the three solutions the torque balance equation (2.1) is made time-dependent by expressing the change in angular momentum as $\zeta\frac{dv}{dt}$ (with ζ being related to the moment of inertia) and leads to $\zeta\frac{dv}{dt} = -\mu v + \beta(v) + \gamma = F(v)$. For time-dependent velocities $v(t) = v_S + \xi(t)$ with the steady state solution v_S the function $F(v)$ is linearized with respect to the infinitesimal perturbation $\xi(t)$ and results in $\zeta\frac{d\xi}{dt} = F'(v_S)\xi$. Numerical calculations show, that the derivative $F'(v_S)$ at the middle branch is always greater than zero and therefore the corresponding v_S is an unstable solution as expected.

When $M > M_+$ the solution jumps from the slow branch to the fast branch. This transition involves hysteresis. Indeed, if M is decreased, the transition back to the slow branch occurs for $M = M_-$ as shown in Fig. 13c and d. The discontinuous transition, which is the main finding of the present work, can be understood as a breakdown of blocking due to the action of the Lorentz forces. Consider a system which is on the slow branch, for instance at $\varepsilon = -0.22$, $P = 30$, $M = 0.7$ (cf. Fig. 13c). According to our discussion of the nonmagnetic problem, this corresponds to a situation where the system is close to stable stratification with a temperature distribution similar to that of inset 2 in Fig. 4a. If the velocity is increased by a sufficiently high amount $\delta V > 0$ due to some external perturbation, less heat will be taken up by the fluid in the heating section. Consequently, less hot fluid invades the region to the left of cooling section 1, and the torque acting on the fluid increases, thereby reinforcing the initial perturbation. This feedback mechanism results in a jump of the system to the fast branch. On this branch $V \sim M$ as in model A. The jump to the last branch is

accompanied by a jump of the temperatures to a lower "cold" state. The overall parameter dependence of the flow is visualized in Fig. 13e where we plot $V(P,M)$ for $\varepsilon = -0.22$. The most important characteristic of this surface is the point (P_c, M_c, V_c), which we shall refer to as the critical point, at which the discontinuous transition occurs first. Since the structure of this surface is identical for all $\varepsilon < 0$, the one-parameter family of critical points $[P_c(\varepsilon), M_c(\varepsilon), V_c(\varepsilon), T_{Hc}(\varepsilon), T_{C1c}(\varepsilon), T_{C2c}(\varepsilon)]$ plotted in Fig. 14 characterizes the behavior of our system to a large extent. Notice that as ε decreases from 0 to -1, corresponding to an increasing asymmetry of the cooling sections, the critical electric current decreases but the critical magnetic field increases.

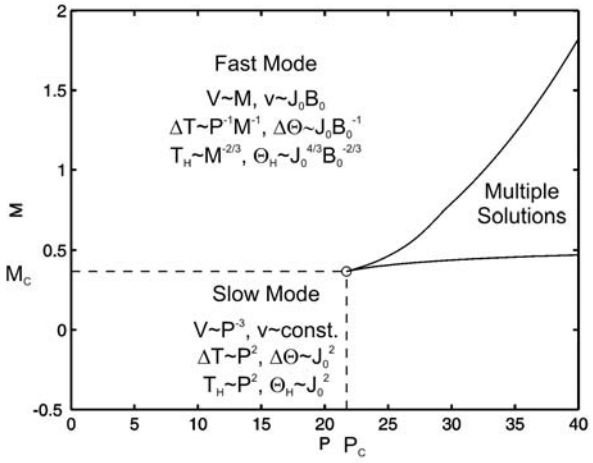

Figure 15 : Phase diagram summarizing the scaling of velocity and temperature in the slow, buoyancy dominated, and in the fast, Lorentz force dominated, regime for $\varepsilon < 0$. MS denotes the parameter region where multiple solutions coexist. Its upper (lower) boundary marks the value of M for which the solution jumps from one mode to the other when M is increased (decreased).

5 Discussion and Conclusions

We have formulated a simple model which permits one to understand how a Lorentz force affects thermal convection in an electrically conducting fluid with high Prandtl number. Our main result is the identification of a discontinuous transition between a slow mode (with higher temperature) and a fast mode (with lower temperature) which occurs for $P > P_c(\varepsilon)$ and has the form of a subcritical bifurcation as a function of the magnetic field. The key mechanism for this effect is that the Lorentz force leads to a breakdown of stable stratification.

Fig. 15 summarizes the behavior of our system in the two-dimensional space of control parameters (P,M) for the case $\varepsilon < 0$ together with the scaling laws for the velocity and temperature. In the slow mode $M \ll 1$ the velocity is independent of the electric current and the magnetic field, while the temperatures increase as J_0^2. On the other hand, in the fast mode the velocity is proportional to the Lorentz force density. The scaling laws for $\Delta\theta$ and θ_H show that the magnetic field does not only affect the velocity but also the heat transfer. The cusp to the right of the critical point represents the region where both fast and slow modes can coexist. Although the scaling relations have been obtained from a simple one-dimensional model, they reflect the competition between the buoyancy and Lorentz force and are therefore believed to hold in more complex geometries with practical relevance as well.

In order to demonstrate that most practically relevant flows have $P > P_c$ and are therefore located in the region where the transition to the fast mode is discontinuous, let us translate the nondimensional values of the critical parameters into physical quantities. For $\varepsilon = -0.96$ we have $P_c = 2.22$, $M_c = 1.73$, $V_c = 0.340$, $T_{Hc} = 0.576$ (cf. Fig. 14). With the parameters of the room temperature model substance (cf. Table 1) this translates into the critical values $J_{0c} = 0.0451 A/cm^2$, $B_{0c} = 0.287T$, $v_c = 0.0355 mm/s$, $\theta_{Hc} = 51.7K$, while for the glass melt we have $J_{0c} = 1.16 A/cm^2$, $B_{0c} = 0.0118mT$, $v_c = 0.0233 mm/s$, $\theta_{Hc} = 229K$. These data can be interpreted in two different ways. Firstly, as soon as the electric current density is higher than J_{0c}, the transition from slow to fast flow takes place discontinuously when the magnetic field exceeds a value of the order B_{0c}. Secondly, if a system is heated such that its temperature is higher than θ_{Hc} above the ambient temperature T_0, then the velocity is a discontinuous function of B_0. Notice that J_{0c} for the glass melt is of the order $0.1 A/cm^2$ which is a typical value of electric current densities in all-electric glass furnaces, and that the minimum required rate of overheating is only $229K$. We can conclude from these figures that all-electric glass melting furnaces operate in a parameter range which is characterized by $P > P_c$ and are therefore susceptible to comparatively weak Lorentz forces.

The general formulas for the dimensional critical parameters are readily derived from the definitions (3.14) and

(3.15) as

$$J_{0c} = 8\kappa L_c \left(\frac{P_c}{c_T d}\right)^3 \left(\frac{\pi\rho_0 \nu c_p \sigma}{\alpha g L_H}\right)^{1/2} \tag{51}$$

$$B_{0c} = \frac{8RM_c}{d}\left(\frac{\pi\rho_0\nu\alpha g}{L_H c_p \sigma}\right)^{1/2} \tag{52}$$

from which

$$v_c = \frac{dJ_{0c}V_c}{8}\left(\frac{\alpha g L_H}{\pi\rho_0\nu c_p\sigma}\right)^{1/2} \tag{53}$$

$$\theta_{Hc} = T_{Hc}\left(\frac{64\pi^2 J_0^4 L_H^2 \nu}{\kappa L_C c_T^3 \rho_0^2 c_p^2 \sigma^2 \alpha g}\right)^{1/3} \tag{54}$$

follow. It is interesting to consider how the critical parameters scale with the size of the system. If all length scales are multiplied with a scaling factor s, the critical parameters are found to behave as

$$J_{0c} \sim s^{-3/2} \tag{55}$$

$$B_{0c} \sim s^{-1/2} \tag{56}$$

$$v_c \sim s^{3/2} \tag{57}$$

$$\theta_{Hc} \sim s^{1/3} \tag{58}$$

Moreover, the critical Lorentz force density $F_{0c} = J_{0c}B_{0c}$ obeys $F_{0c} \sim s^{-3}$ implying that with increasing system size the system becomes increasingly susceptible to Lorentz forces. This observation suggests that electromagnetic forces might be quite effective in controlling glass melt flows in large enclosures. We parenthetically note that electromagnetic boundary layer control in another poorly conducting fluid - namely seawater - has attracted a considerable research interest (Gailitis & Lielausis 1961, Tsinober & Shtern 1967, Tsinober 1990). Even if there is no externally applied magnetic field in glass processing, the magnetic field of the current itself scales as $B_0 \sim J_0$. This implies that a system with natural Lorentz forces moves along a curve $M \sim P^3$ in the (P,M) plane and thereby is likely to penetrate the multiple state domain shown in Fig. 15. Consequently, it is likely that it may often be important to include Lorentz forces in simulations of all-electric glass furnaces.

Finally, a brief comment on the limits of validity of the present theory is in order. We have neglected the internal heat transfer by radiation as well as the temperature dependence of both η and σ, which limits the validity of our approach to small temperature variations as in the interior of a glass melting furnace. However, the present model can be modified so as to incorporate these effects at only slightly increased mathematical complexity as has been demonstrated by Lange & Loch 2002 for (nonmagnetic) flow of a glass melt in a pipe. A similar statement is true for inertial effects which could be taken into account by using the full expression for the friction coefficient $c_f(v)$ rather than the laminar expression. Also, more general heat transfer models including experimentally determined heat transfer coefficients could be used.

Acknowledgement: This work was supported by the Deutsche Forschungsgemeinschaft in frame of the Forschergruppe Magnetofluiddynamik. We are grateful to O. R. Hofmann, Ch. Karcher, Y.B. Kolesnikov and U. Lange for useful discussions.

References

Beerkens R. (2002): Modeling of the melting process in industrial glass furnaces. in: *Mathematical simulation in glass technology, Schott Series on Glass and Glass Ceramics, eds. D. Krause & H. Loch*, Springer Verlag Berlin, 17–73.

Bojarevics V.; Y. Freibergs, E.I. Shilova, E.V.Shcherbinin (1988): Electrically Induced Vortical Flows. *Kluwer Academic Publishers*, Dordrecht.

Ching E.S.C. (1997): Heat flux and shear rate in turbulent convection, *Phys. Rev. E*, **55**, 1189–1192.

Choudhary M.K. (1995): A modeling study of flow and heat transfer in the vicinity of an electrode. *Proc. XVII Int. Congress on Glass*, **6**, (Chinese Ceram. Soc. Beijing), 100–107.

Creveling H.F.; De Paz J.F.; Baladi J.Y.; Schoenhals R.J. (1975): Stability characteristics of a single-phase convection loop, *J. Fluid Mech.*, **67**, 65–84.

Davidson P.A. (1999): Magnetohydrodynamics in materials processing, *Annu. Rev. Fluid Mech.*, **31**, 373–300.

Davidson P.A.; Lindsay R. (1998): Stability of interfacial waves in aluminium reduction cells, *J. Fluid Mech.*, **32**, 273–295.

Davidson P.A. (2001): An Introduction to Magnetohydrodynamics, *Cambridge University Press.*

Davis S.H.; Roppo M.N. (1987): Coupled Lorenz oszillators, *Physica D*, **24**, 226–242.

Table 4 : List of symbols

Symbol	Unit	Meaning
B_0	[T]	magnetic field density
c_f	[1]	friction factor
c_P	[kJ kg^{-1} K^{-1}]	specific heat capacity
c_T	[1]	numerical value
c_V	[1]	friction coefficient
d	[m]	inner diameter of the loop
g	[m s^2]	acceleration of gravity
J_0	[A m^{-2}]	electric current density
L_H	[m]	length of the heating section
L_C	[m]	length of the cooling section
M	[1]	non-dimensional lorentz force parameter
P	[1]	modified Peclet number
R	[m]	radius of the loop
T	[1]	non-dimensional temperature
v	[m s^{-2}]	velocity
v_0	[m s^{-2}]	norm velocity
V	[1]	non-dimensional velocity
α	[K^{-1}]	coefficient of expansion
β	[N m]	buoyancy torque
γ	[N m]	lorentz torque
ε	[1]	length scaling parameter of the cooling sections in Model B
κ	[m^2 s^{-1}]	thermal diffusivity
μ	[N s^{-1}]	friction coefficient
ν	[m^2 s^{-1}]	dynamic viscosity
ρ	[kg m^{-3}]	density
σ	[Ω^{-1} m^{-1}]	electrical conductivity
θ	[K]	temperature
θ_0	[K]	norm temperature
φ	[1]	angle of the loop

Ehrhard P.; Karcher C.; Müller U. (1989): Dynamical behaviour of natural convection in a double loop system, *Exp. Heat Transfer*, **2**, 13–26.

Ehrhard P.; Müller (1990): Dynamical behaviour of natural convection in a single-phase loop, *J. Fluid Mech.*, **217**, 487-518.

Gailitis A.; Lielausis O. (1961): On the possibility of drag reduction of a at plate in an electrolyte, *Appl. Magnetohydrodynamics, Trudy Inst. Fis. AN Latv. SSR* , **12**, 143.

Grossmann S.; Lohse D. (2000): Scaling in thermal convection: a unifying theory, *J. Fluid Mech.*, **407**, 27–56.

Grossmann S.; Lohse D. (2003): On geometry effects in Rayleigh–Benard convection, *J. Fluid Mech.*, **486**, 105–114.

Hofmann O.R.; Philip G. (1992): Importance of the Lorentz force in electrically heated glass melts *Glastech. Ber.* **65**, 142–149.

Hofmann O.R.; Thess A. (2002): Electromagnetic control of glass melt flows: A new branch of applied magnetohydrodynamics? (in German) *Glas-Ingenieur* **1**, 39–45.

Illig H.J, Linz H.J.; Michelsen C.E. (1978): Beitrag zur wissenschaftlich-technischen Beschreibung der vollelektrischen Schmelze von Glas, PhD dissertation *Bergakademie Freiberg, Germany*

Keller J.B. (1966): Periodic oscillations in a model of thermal convection , *J. Fluid Mech.*, **26**, 599–606.

Krause D. & Loch H. (eds.) (2002): Mathematical simulation in glass technology *Schott Series on Glass and Ceramics* Springer-Verlag Berlin.

Lange U.; Loch H. (2002): Instabilities and stabilization of glass pipe flow. in: *Mathematical simulation in glass technology, Schott Series on Glass and Glass Ceramics, eds. D. Krause & H. Loch*, Springer Verlag Berlin, 193–208.

Osmanis A.D.; Snijedze A.K.; Aglitis A.M. (1987): Influence of electromagnetic stirring of glass melts (in Russian)*Proceedings of the 12th Riga Symposium on Magnetohydrodynamics*, Salaspils, USSR, 179–183.

Prasad R.S.O.; Mukhopadhyay A.; Dutta A. (1999): Implementation of a glass batch-melting model in the general purpose three-dimensional CFD code FLUENT. *Proc. V Int. Seminar on Mathematical Simulation in Glass Melting*, June 17-18, 1999, Horni-Becva, Czech Republic, 1–9.

Shraiman B.; Siggia E. (1990): Heat transport in high-Rayleigh number convection. *Phys. Rev. A* **42**, 3650–3653.

Siggia E.D. (1994): High Rayleigh number thermal convection, *Annu. Rev. Fluid Mech.*, **26**, 137–168.

Stanek J. (1977): Electric melting of glass. *Elsevier*, Amsterdam, Oxford, New York.

Thess A.; Conrad G.; Halbedel B.; Hülsenberg D.; Kolesnikov Y.; Lüdtke U. (2003): Electromagnetic stirring of glass melts *Proceedings of the International Congress on Electromagnetic Processing of Materials*, 13–17 October 2003, Lyon, France.

Tsinober A. B.; Shtern A. G. (1967): Possibility of increasing the flow stability in a boundary layer by means of crossed electric and magnetic fields, *Magnetohydrodynamics*, **3**, 103.

Tsinober A.B. (1990): MHD-Drag Reduction. In: Viscous Drag Reduction in Boundary Layers, *AIAA "Progress in Aeronautics and Astronautics" series*, eds. Bushnell D.M. and Hefner, **123**, 327–349.

Welander P. (1967): On the oscillatory instability of a differentially heated fluid loop, *J. Fluid Mech.*, **29**, 17–30.

White F.M. (2002): Fluid Mechanics, *Mc Graw Hill.*

Wylie J.W.; Lister J.L. (1995): The effects of temperature-dependent viscosity on flow in a cooled channel with applications to basaltic fissure eruptions, *J. Fluid Mech.*, **305**, 239–261.

Wylie J.W.; Lister J.L. (1998): Stability and straining flow with surface cooling and temperature-dependent viscosity, *J. Fluid Mech.*, **365**, 269–281.

Yorke J.A.; Yorke E.D.; Mallet-Paret J. (1987): Lorenz-like chaos in a partial differential equation for a heated fluid loop, *Physica D*, **24**, 279–291.